

Catalysis Science & Technology

Accepted Manuscript

This article can be cited before page numbers have been issued, to do this please use: W. R. Heinz, R. Junk, I. Aguirrezabal Telleria, B. Bueken, H. Bunzen, T. Gözl, M. Cokoja, D. E. De Vos and R. A. Fischer, *Catal. Sci. Technol.*, 2020, DOI: 10.1039/D0CY01479F.



This is an Accepted Manuscript, which has been through the Royal Society of Chemistry peer review process and has been accepted for publication.

Accepted Manuscripts are published online shortly after acceptance, before technical editing, formatting and proof reading. Using this free service, authors can make their results available to the community, in citable form, before we publish the edited article. We will replace this Accepted Manuscript with the edited and formatted Advance Article as soon as it is available.

You can find more information about Accepted Manuscripts in the [Information for Authors](#).

Please note that technical editing may introduce minor changes to the text and/or graphics, which may alter content. The journal's standard [Terms & Conditions](#) and the [Ethical guidelines](#) still apply. In no event shall the Royal Society of Chemistry be held responsible for any errors or omissions in this Accepted Manuscript or any consequences arising from the use of any information it contains.

ARTICLE

Thermal Defect Engineering of Precious Group Metal-Organic Frameworks: Impact on the Catalytic Cyclopropanation Reaction

Werner R. Heinz,^a Raphael Junk,^a Iker Agirrezabal-Telleria,^b Bart Bueken,^c Hana Bunzen,^d Thorsten Götz,^a Mirza Cokoja,^a Dirk De Vos,^c and Roland A. Fischer^{*a}

Received 00th January 20xx,
Accepted 00th January 20xx

DOI: 10.1039/x0xx00000x

We report on the engineering of defects in precious group metal (PGM)-based HKUST-1 (Hong Kong University of Science and Technology) analogues (Rh^{III}, Ru^{II,III}, Ru^{II,III}) and the ramification on the catalytic activity by using the cyclopropanation of styrene with ethyl diazoacetate (EDA) as analytical probe to investigate complex metal-organic framework (MOF) structures. We have characterized the active sites within the extended frameworks by their activity, product distribution and stereoselectivity. The role of the metal, its oxidation state and the availability of open metal sites are elucidated. With a set of 17 samples including reference to Cu-HKUST-1, metal nanoparticles and existing literature, conclusions on the tuneability of paddlewheel complexes within self-supported porous and crystalline frameworks are presented. In particular, additional axial ligands (OAc/Cl) accounting for charge compensation at the mixed-valent Ru^{II,III} nodes seem responsible for side-product formation during catalysis. Thermal defect-engineering allows for controlled and preferential removal of those axial ligands accompanied by reduction of the average metal oxidation state. This enhances the number of open metal sites (OMS) and the catalytic activity as well as improves the chemoselectivity towards cyclopropanes. The preference towards formation of *trans*-cyclopropane is assigned to the steric crowding of the paddlewheel moiety. This diastereoselectivity gradually diminishes with rising defectiveness of the PGM-HKUST-1 analogues featuring modified paddlewheel nodes.

Introduction

The transition metal catalyzed cyclopropanation (CP) of olefins is a well-established reaction in molecular catalysis. From the first report of Rh₂(OAc)₄ almost fifty years ago, its underlying lantern-like binuclear “paddlewheel” structure (PW, see Figure 1) has ascended and now represents the benchmark catalyst system for this reaction.¹⁻³ Many efforts have been made and libraries of new ligands (all kinds of carboxylates, carboxamidates, phosphonates and others) were created to achieve higher activities but also to access chemo-, diastereo- and even enantioselectivity.⁴ Consequently, deepest mechanistic comprehension of important parameters for this and other related reactions involving transition metal carbenoid species is available in literature.^{2, 5-9} Side-products resulting from homocoupling of two carbenes or from C–H activation are

known to occur.¹⁰⁻¹⁵ The latter reaction requires two open metal sites (OMS) at the metal center and yields linear allyl species which are further denoted as linear products. A

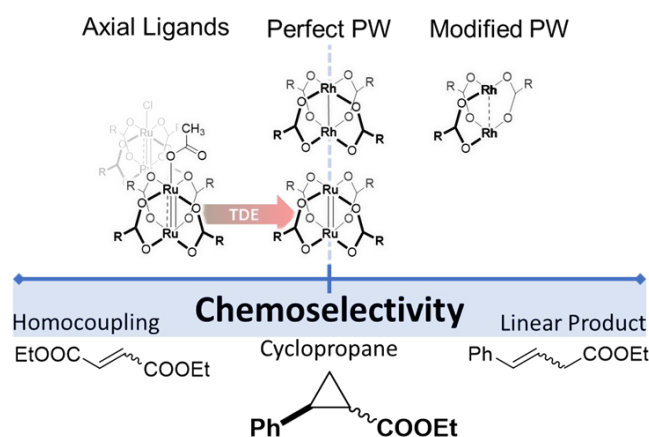


Figure 1: Concept of this work: The carbene-transfer catalysis and its catalytic characteristics such as activity, chemo- and diastereoselectivity can be exploited as analytical tools to investigate compositionally complex porous catalyst materials (here precious metal-based HKUST-1 analogues) comprising different kinds of paddlewheel structures. Putative assignment of the PW-types (mixed-valent with axial ligands, perfect or modified) with their catalytic chemoselectivity: Middle: Cyclopropanes; Left: Tendency to form homocoupling products; Right: Tendency to form linear products. During TDE, the mixed-valent Ru-PWs undergo axial ligand removal and reduction towards univalent PWs leading to improved CP selectivity. In contrast, Rh-HKUST-1 comprises mixtures of perfect and defective PWs being mostly unaffected by TDE. The organic residue R can be either CH₃ as modulator derived acetate defect or C₆H₃O₄ as trimesate linker. The full structural complexity is highlighted in Scheme S1 and S2.

^aChair of Inorganic and Metal-Organic Chemistry, Department of Chemistry and Catalysis Research Center, Technical University of Munich, Ernst-Otto-Fischer-Straße 1, D-85747 Garching bei München, Germany. E-mail: roland.fischer@tum.de

^bDepartment of Chemical and Environmental Engineering, Engineering School of the University of the Basque Country (UPV/EHU), Plaza Torres Quevedo 1, 48013 Bilbao, Spain.

^cCentre for Membrane Separations, Adsorption, Catalysis and Spectroscopy for Sustainable Solutions, Department of Microbial and Molecular Systems (M2S), KU Leuven, Celestijnenlaan 200F p.o. box 2461, 3001 Leuven, Belgium.

^dChair of Solid State and Materials Chemistry, Institute of Physics, University of Augsburg, Universitätsstraße 1, D-86159 Augsburg, Germany.

*Corresponding author

Electronic Supplementary Information (ESI) available: See DOI: 10.1039/x0xx00000x

mechanistic summary assisting the conclusions from this paper is provided in the supporting information (ESI).

One possible strategy to overcome the limitations of isolated complexes in homogeneous catalysis (e.g. catalyst separation, recycling) is their immobilization in solid materials.¹⁶⁻²¹ Consequently, the performance of some related materials has been studied in the cyclopropanation of styrene with ethyl diazoacetate (EDA) as test reaction.^{12, 22-25} Many of these reports focused on the influence of tuning the local structure of the catalytically active centers on the catalytic activity. For instance, *Buntkowsky et al.* studied rhodium-based coordination polymers with 2D sheet structure comprising Rh₂-PWs interconnected with terephthalate linkers regarding the impact of linker side chains in this reaction.²³⁻²⁵ *Corma et al.* reported Cu₃(BTC)₂ (BTC = 1,3,5-benzene tricarboxylate; aka HKUST-1, Hong Kong University of Science and Technology), to exhibit good activity and stability in this CP.²⁶ More recently, we have found unexpectedly high diastereomeric selectivity for the cyclopropanation of substituted styrenes catalyzed by metalated porphyrin-based MOFs as a result of pore confinement and directing effects by adjacent metal nodes.¹² The CP-enantioselectivity is intrinsically more difficult to control with MOF catalysts.

In recent years, the perception of defects in MOFs has changed significantly as defective sites often dominate material properties relevant for manifold applications such as catalysis, gas sorption and separation or electric and ionic conductivity.²⁷⁻³⁰ Thus, ways to control the defect formation or even to intentionally introduce defects into MOFs either *de novo* during synthesis or postsynthetically have been developed. Recently, we established a process for thermal defect-engineering (TDE) of MOFs as novel way to postsynthetically introduce defects into precious-group metal (PGM)-based analogues of the archetypical PW-based HKUST-1 structure.³¹ In contrast to their structural parent (Cu-HKUST-1), the PGM analogues (Ru, Rh and mixed-metal RuRh) feature high compositional complexity due to their pronounced defectiveness and are challenging to characterize on the atomic scale. Many common techniques such as single-crystal X-ray diffraction (SC-XRD), compositional analysis after acid digestion, X-ray photoelectron (XPS) and energy-dispersive X-ray spectroscopy (EDX) are not applicable or do not fulfil their typical potential in these microcrystalline, highly stable PGM-based materials.

In contrast to previous studies on the catalytic CP seeking for ever increasing catalyst performance, and in the light of our previous reports on the influence of macroscopic structural modifications of MOFs,³¹ we intend to demonstrate an opposite strategy herein. In this proof-of-concept study, we aspire to probe the local catalyst structure (and its changes) for a better structural comprehension by the CP reaction and its characteristics (such as activity and selectivity as highlighted in Figure 1). In other words, we were motivated to exploit the well-established comprehension of the manifold reaction characteristics as analytical probe to access the complex defect chemistry of isostructural TDE-PGM-HKUST-1 analogues. The specific impact of the metal choice, its oxidation state and

defectiveness (as modified by TDE) are investigated, and conclusions on the tuneability are drawn. DOI: 10.1039/DOCY01479F

Experimental

General considerations about working procedures, used chemicals and solvents as well as instrumental details are listed in the supporting information. Spectra and analytical data regarding MOF characterization are also provided.

Synthesis of MOF samples

The synthesis of the pristine precious-metal MOFs was conducted in analogy to the literature procedures for Ru₃(BTC)₂ (univalent), Ru₃(BTC)₂Y_{1.5} (Y = Cl/OAc; mixed-valent) and Ru_xRh_{3-x}(BTC)₂Y_{x/2} (mixed-metal).³²⁻³⁵ Cu₃(BTC)₂ was synthesized according to a room temperature literature procedure.³⁶ Defective samples were produced from pristine materials by means of a TGA-based thermal treatment within an argon-filled glovebox allowing access to predefined and reproducible degrees of additional defectiveness within the samples. Weight-losses of 5.5%, 10% and 15% were chosen to obtain samples denoted 10%D, 20%D and 30%D (D= defects) according to their rough defect amounts. For defective samples, a (XX/YY) nomenclature was used, referring to XX% rhodium fraction within the bimetallic MOF samples of Ru and Rh. YY% refers to the post-synthetically introduced defect amount (0% for the pristine and ≈10%, 20% and 30% for defective samples). Metal nanoparticles were produced through complete thermal decomposition of respective MOF samples.

Basic characterization data (PXRD, TGA, EA, N₂ physisorption, IR and Raman spectroscopy) of all MOF samples is given in the ESI.

HR-TEM and Elemental Mapping

HR-TEM, STEM micrographs and EDS elemental mappings were recorded with a JEM NEOARM microscope (JEOL) with a cold FEG electron source operated at 200 kV. Samples were prepared by depositing a drop of the crystalline products dispersed in ethanol onto carbon-coated copper grids (200 mesh) and dried in air. Images of all samples are displayed in Figure 2 and S21-23. Elemental maps are displayed in Figures 2 and S24-25.

CO Titration of OMS

TGA-based OMS titration experiments using CO were conducted in the following manner: In a stream of Ar (40 mL min⁻¹), the MOF sample was heated to either 150 or 300 °C in Ar and successively to 150 °C in H₂ for activation or defect generation. After cool-down to ambient temperature, the residual weight was taken as reference and further monitored during additional CO dosage with increasing flow rates (5, 10 and 15 mL min⁻¹). Calculated CO uptakes (Table S3) refer to mass peak values during CO dosage. All related graphs, temperature programs and respective weight curves are displayed in Figures S16-20.

Catalysis experiments

Cyclopropanation reactions were carried out with an optimized procedure. Either each 5 mg ("same weight") or 1.32 mol-% (with respect to EDA; "same equivalents") of finely ground activated MOF samples was weighed in screw-capped vials with septa within a solvent-free argon-filled glovebox. A cross-shaped stirring bar was added, and the vials were tightly closed prior to the transfer out of the glovebox. A solution of 0.5 mL styrene in 0.5 mL dichloromethane was added and the mixture was vigorously stirred to obtain a homogeneous dispersion. For the entire reaction, a stirring rate of 150 min⁻¹ was set. Utilizing a syringe pump, a solution comprising 2.4 mL dichloromethane, 2.4 mL styrene, 0.2 mL toluene and 0.2 mL EDA was added with a rate of 0.087 mL s⁻¹ to achieve a total addition time of one hour. An additional cannula accounted for pressure release upon nitrogen formation. Samples of 0.1 mL were taken at the respective reaction time (t = 0 at the end of the addition time), diluted in 0.7 mL dichloromethane and syringe filtered (0.2 μm pores). Reaction conversions and selectivities were determined by GC (HP-5 column) with flame ionization detection. Product identification was performed according to earlier reports.^{12, 15} For the hot filtration test, the catalytic procedure was conducted accordingly with separation of a sample of 1 mL and successive syringe filtration into a similarly stirred reaction vial including continuous sampling. Reusability was verified by repeated use of MOF material in five consecutive runs with sampling after 4 h each. The catalyst was centrifuged afterwards, and a fresh EDA dose was added according to the general procedure. The small residual amount was used for PXRD after the fifth run. Formulae for TOF and selectivity calculations are provided in the ESI.

Results and Discussion

Synthesis & Characterization of Thermal Defect-Engineered MOFs

Modulated hydrothermal synthesis utilizing the concept of the controlled secondary building unit approach was chosen to produce precious metal-based HKUST-1 derivatives of ruthenium, rhodium, and a bimetallic variant. Therein, the ruthenium dimers in paddlewheel (PW) structures possess a mixed valency (II,III) while rhodium PWs are univalent (II,II). In the mixed-valent Ru case, one additional axially bound ligand (acetate or chloride) per PW accounts for charge compensation. The selected oxidation states represent the air-stable configurations and accord to the chosen precursors Ru₂(OAc)₄Cl and Rh₂(OAc)₄. In the following, an (X / Y) notation is used to describe the samples with X referring to the fraction of rhodium within the metal nodes (0, 50, 100% with respect to the Rh^{II,III} to Ru^{II,III} ratio) and Y describing the defectiveness (0, 10, 20, 30%) introduced postsynthetically via TDE. Note that Y merely qualitatively describes the postsynthetically introduced defect amounts and should simplify the exact results derived from various experimental data, calculation approaches and different pristine MOF samples. A detailed description of definitions and precise calculations of the defectiveness is given in the ESI (see Table S2). As introduced in our earlier report,³¹ the controlled

thermal defect-engineering (TDE) with successive isothermal steps (see Figure S1) was performed with a TGA-MS setup within a glovebox. This allows to produce and handle TDE-MOF samples with unique gravimetric process control over the progress of thermal annealing and to prevent these highly reactive samples from undesired (and uncontrolled) deactivation in air or moisture. For TDE-MOF sample synthesis, precise weight losses of 5.5, 10 and 15 wt.% with respect to the activated pristine PGM-MOFs were targeted. To ensure high reproducibility, initial sample weights (100 wt.%) were referenced to the stable weights at 150 °C isothermal treatment.

All samples – pristine and TDE-MOFs – were characterized with PXRD, elemental analysis, FT-IR, Raman, nitrogen physisorption (including pore size analysis) and thermogravimetry. All related patterns, spectra and isotherms are displayed in the supporting information (see the ESI, Figures S2-15 and Table S1). The performed analyses suggest that TDE does not negatively affect the crystallinity of the isostructural samples. In Rh-based MOFs, however, upon TDE, increasing nanoparticle (NP) formation can be observed in the XRD patterns. Information derived from vibrational spectroscopy suggests decarboxylation of BTC linkers forming isophthalate and the removal of axial and equatorial acetate (modulator) ligands. Pristine mixed-valent ruthenium PWs typically possess one additional axial ligand for charge compensation being either acetate or chloride. During TDE, the axial acetates are readily removed providing access to univalent Ru^{II,III} sites with two open metal sites (OMS) per PW. In contrast, the axial chloride ligands mostly remain strongly bound. Regarding the porous structure, all samples exhibit and retain their high porosity during TDE with slight shifts towards larger pore sizes because of partial pore wall removal during TDE. Elemental analysis data, with some assumptions, allow for the determination of empirical sum formulae. These also support the removal of organic constituents during TDE with a preference towards acetate removal. As a result, the mean metal valences decrease due to the formation of modified PWs. PXRD, EA, IR, Raman and BET data are provided in the Supporting Information.

To visualize the morphology and crystallite sizes of the produced MOF samples, high-resolution transmission electron microscopy (HR-TEM) with elemental mapping was performed. Representative images of selected samples are displayed in Figure 2. NPs can be identified neither in the pristine Ru-MOF (0/0) nor in the respective TDE-MOFs (0/30) (top block, left images). In contrast, clusters of NPs are already present in the pristine Rh-MOF (100/0) sample migrating and agglomerating into larger NPs upon TDE (100/30). The pristine mixed-metal MOF sample (50/0) does not contain NPs but small NPs emerge from 20% defects on. These findings are supported by the PXRD data mentioned earlier (see the ESI, Figures S2 and S3). The elemental maps displayed in Figure 2 indicate the bimetallic nature of both the pristine (50/0) and the TDE-RuRh-MOF (50/30) and support the absence of demixing phenomena and overall preserved structural integrity (confirmed by PXRD) during TDE.

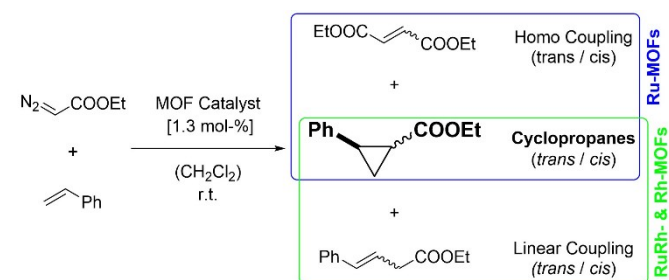
To quantify the catalytically relevant number of OMS, we designed a TGA-based titration experiment utilizing carbon monoxide as a probe molecule (for selected samples, see Figure

S16). First, each pristine MOF sample was treated at higher temperatures to fully desolvate the axial coordination sites or to thermally induce defects into the materials. At ambient temperature, a diluted stream of CO was dosed through the chamber and the respective weight gain was monitored (see Table S3). Gravimetric numbers were converted into molecules CO per PW assuming stoichiometric sorption of 1 CO per metal site as concluded from earlier reports.³¹ For instance, thermal treatment leads to an increase from 0.72 CO per PW (after 150 °C) to 1.86 CO per PW (after 300 °C treatment) of the Ru^{II,III} sample. Pretreated at 300 °C, 0.59 CO adsorb at each Rh PW, while it is 0.97 CO per Ru^{II,III}-PW after the identical defect creating treatment. The respective thermogram and all values are given in the ESI confirming the redox flexibility of ruthenium samples with increasing number of OMS upon thermal treatments.

TDE-MOFs as Catalysts for the Cyclopropanation of Styrene

As introduced above, the CP of styrene with ethyl diazoacetate (EDA) was studied intensively in molecular catalysis. Related reaction characteristics such as activity, chemoselectivity and diastereoselectivity predictably correlate with the number (and reactivity) of OMS, the electronic environment of the PW (oxidation state, presence/absence of axial counterions) and its steric properties (ideal/defective PW). With this solid literature basis, we wanted to use the reaction as a probe to obtain deeper insights into the complex structure of PGM-MOFs and their thermally defect-engineered derivatives (TDE-MOFs), and to investigate the possibilities of catalyst improvement for this reaction. Previous analysis of the related materials was used to validate the results of this novel approach.

First, a general procedure for the CP was developed using a low catalyst loading of only 1.3 mol-% related to the limiting EDA amount. Similar to earlier reports, a large excess of olefin was used and slow addition of the EDA solution used to suppress a homocoupling reaction between the formed carbene species and a second EDA molecule, which then results in diethyl fumarate or maleate as side products.^{12, 37, 38} The reaction was performed by suspending the solid MOF catalyst in dichloromethane at ambient temperature for reasons of experimental convenience and comparability with previous works. Within this study, three different groups of products



Scheme 1: Overview of the reaction products from the reaction of styrene with EDA catalyzed by MOF catalysts. A molar ratio of 0.013 : 1 : 15.66 with respect to metal, EDA and styrene was applied. The catalyst was suspended in a mixture of 0.5 mL styrene and 0.5 mL dichloromethane for 15 min until a solution of 2.1 mL styrene, 2.1 mL dichloromethane, 0.1 mL toluene and 0.1 mL EDA was added via a syringe pump over one hour. Sampling was started at the end of addition.

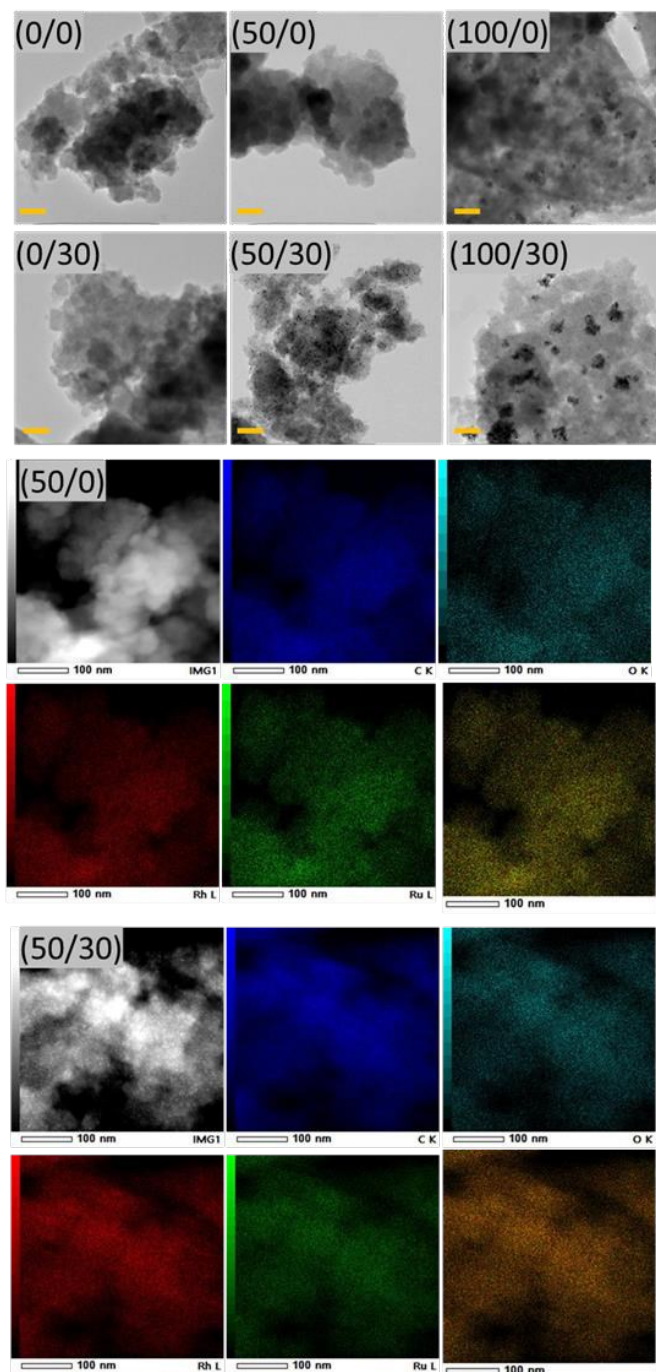


Figure 2: Top block: HR-TEM images of representative samples: left: pristine (0/0) and most defective Ru-MOF (0/30), middle: pristine (50/0) and most defective RuRh-MOF (50/30), right: pristine (100/0) and most defective Rh-MOF (100/30). Yellow scale bars represent 50 nm. TDE does not impose topological changes or NP formation in Ru-MOF. In contrast, Rh-containing MOFs exhibit increasing NP formation. Note: The (100/0) pristine sample already contains NPs from synthesis. Middle and bottom blocks: Selected dark field STEM images of representative particles of (50/0) (middle) and (50/30) (bottom) and the corresponding EDS elemental mapping for C, O, Rh, Ru and the overlaid Ru/Rh signals. White scale bars represent 100 nm. The maps support the bimetallic nature of the mixed-metal particles even upon NP formation during TDE. Maps for pure Rh-based samples are provided in Figures S23-24.

were observed (see Figure 1 & Scheme 1). The desired *cis* and *trans*-cyclopropanes ethyl 2-phenylcyclopropane-1-carboxylate are the main reaction products. As side products, the aforementioned homocoupling products but also a couple of linear allyl species resulting from carbene C-H insertion are observed in some reactions (see Figure 1). Note, that the selectivity of this reaction is generally unaffected by conversion, temperature, solvent or catalyst loading. Therefore, chemoselectivities after 24 h are compared in Figure 4.

Investigation of the Pristine MOF Catalysts All investigated PGM-MOFs exhibit catalytic activity for the cyclopropanation of styrene with EDA. Turnover frequencies (TOFs) representing the activity of the materials are displayed in Figure 3 for all PGM-MOFs (time-conversion graphs for early data points are provided in Figure S26). At first, we compared results obtained with identical MOF catalyst loadings of 5 mg each (metal contents range between 37 and 48%, detailed values are given in the ESI). While the activity of the pristine Ru-MOF is comparably low with 40% conversion after 4 h, the mixed-metal RuRh (50/0) sample reaches 92% after 4 h. An even greater activity can be observed for the pure Rh-MOF reaching quantitative conversion of EDA already after 1 h. Normalized to the metal content, the initial activities are rather comparable for both pristine RuRh- and Rh-MOF (see Figure 3, bottom graph). Note, that a reference experiment with molecular $\text{Rh}_2(\text{OAc})_4$ gave full conversion already at the first sampling (0 min) at the end of the EDA addition. Thus, the experimental procedure applied herein limits the calculated TOF for $\text{Rh}_2(\text{OAc})_4$ to 145 h^{-1} .

Looking at the product distribution, significant differences can be observed within the used metals as can be seen in Figure 4. A schematic overview of the different PW-types (mixed-valent, univalent, modified) and their associated selectivity is given in Figure 1. Interestingly, Ru-MOF forms large amounts of homocoupling products ($\approx 30\%$) with CP selectivities of $\approx 64\text{--}68\%$. Rh-containing MOFs do not induce the formation of the homocoupling product. However, besides the cyclopropanes, different products that stem from the coupling of styrene with EDA are observed instead. Linear allyl species (15–18% selectivity) are formed. These could potentially arise from a C-H insertion reaction of the carbene species into olefinic C-H bonds or result from ring opening reactions. The former reaction, often termed “C-H insertion” or “homologation reaction”, has rarely been reported for PW-type catalysts.^{11, 37, 39, 40} Predominantly, isolated ruthenium complexes were found to yield these linear side products also using excessive styrene concentrations.^{11, 13, 15, 41} The molecular $\text{Rh}_2(\text{OAc})_4$ reference did not produce such linear products in detectable amounts under our reaction conditions. In general, for CP to occur, only one available OMS is required for the carbene formation / coordination. The axial position of PW complexes serves this purpose well. All literature reports have in common that the C-H activation requires more space at the metal site allowing for the coordination of both the carbene species and the olefin simultaneously.¹¹ Therefore, we conclude that the formation of the linear allyl species might be catalyzed by modified PWs

(present in missing linker defects, see Figure 1 and Scheme S3).³⁵ In principle, styrene should be capable to coordinate to all types of OMS. At a defective PW, this is one free equatorial position and the two adjacent axial positions. All of them may be coordinated by styrene molecules at the beginning of the reaction. Upon EDA dosing, one axial styrene can be substituted by EDA accompanied by N_2 release and formation of the proposed metal carbenoid species. The adjacent coordination (*cis*) of both styrene and the carbene species at one metal center (such a potential intermediate is displayed in Scheme S3) meets the conditions for the C-H insertion as proposed in the literature.¹¹ Turning to the mixed-metal RuRh-MOF, an almost identical product distribution as for the Rh-MOF can be observed ($\approx 15\%$ linear products; no homocoupling products). Together with the similar activity of both catalyst materials, its catalytic properties seem to be dominated by the rhodium sites.

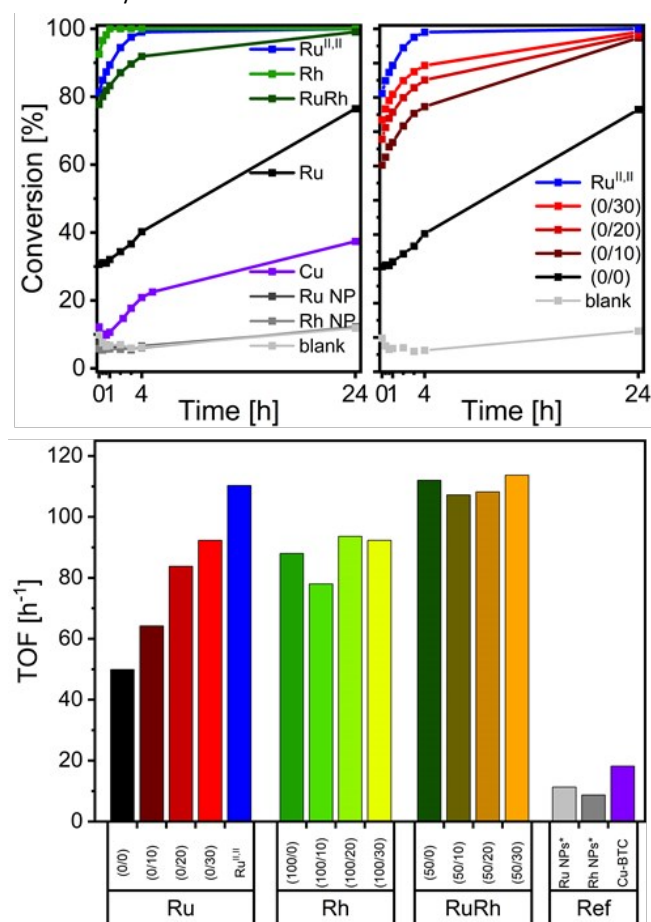


Figure 3: Activity in the cyclopropanation reaction of styrene with EDA. Top left: Time-conversion plots comparing different pristine HKUST-1 analogues of Cu (purple), Ru (mixed-valent (black) and univalent (blue)) and Rh (green) with respective NPs (grey) as catalysts. Top right: Activity comparison of different ruthenium-based MOFs: The moderate activity of the mixed-valent $\text{Ru}^{\text{II,III}}$ MOF (0/0) is strongly enhanced by TDE (0/10 \rightarrow 30) (brown to red curves). Bottom: Overview on turnover frequencies (TOFs) derived from initial conversions and 30 min average reaction time within 1 h for the controlled EDA addition. As can be seen, compared to the reference materials, all PGM-MOFs exhibit high activities and the beneficial effect of TDE to enhance the activity of Ru-MOF by OMS generation can be seen. *Observed conversions are in the range of the uncatalyzed background reaction. The molecular $\text{Rh}_2(\text{OAc})_4$ (not displayed) reached full conversion already at 0 min, thus its TOF is experimentally limited to 145 h^{-1} .

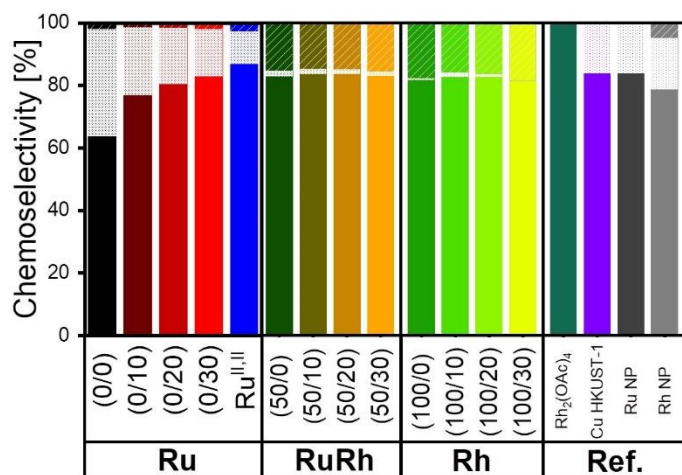


Figure 4: Chemoselectivities for all samples after 24h. The three groups of products are displayed in stacked columns. The bottom bars represent the cyclopropanes (strongly colored), the fractions in the middle (pale) represent the observed homocoupling products. Top bars (cross-hatched) represent the fractions of linear products. Left group: Ru-MOF samples indicate improved chemoselectivity towards CPs and decreasing homocoupling upon TDE indicating the axial ligand removal. Middle left (mixed-metal RuRh-MOFs) and middle right (Rh-MOFs) group: Linear products as side products emerge. TDE has no effect on the chemoselectivity for RuRh- and Rh-based samples. Right group: Reference samples. Note that, the conversion of metal NPs is very low, thus represents merely the uncatalyzed background reaction.

Focusing on the stereoselectivity, the *trans*-isomer is slightly favoured (≈ 64 - 68%) when using "perfect" PWs like Rh₂(OAc)₄ or heterogenized PWs as they are present in Cu-HKUST-1.^{22, 26, 38} As explained in the ESI in detail, the reaction is controlled through the geometry of the PW. As displayed in Figure 5, the resulting diastereoselectivity in HKUST-1 analogues is decreasing in the order Cu \gg Ru $>$ RuRh $>$ Rh. This order is also representing the intrinsic defectiveness of pristine samples resulting from modulated synthesis. Defective PWs presumably miss the directing effects of the steric "wall" formed by the metal and its four equatorial oxygen atom ligators. This is in line with earlier reports on Ru- and Rh-based HKUST-1 analogues featuring increasing amounts of defects.^{34, 35, 42}

Investigation of the TDE-MOF Catalysts Proceeding from the pristine PGM-MOFs towards their thermally treated defective analogues, we performed identical catalytic reactions with all TDE-MOFs and an additional univalent Ru^{II,III} reference sample. In the ruthenium case, TDE clearly increases the catalytic performance as can be seen in both Figure 3 and in the time-conversion plots for the whole series (see Figures 26-29). The strong increase in activity is also visible in more than doubled TOFs (from ≈ 50 h⁻¹ for pristine Ru-MOF over ≈ 92 h⁻¹ for the (0/30) sample towards ≈ 110 h⁻¹ for the Ru^{II,III}-MOF) presented in Figure 3. This activity improvement can be attributed to the removal of the axial acetate ligands providing a higher number of OMS per PW as outlined above. Beyond the observed increase in activity, TDE of Ru-MOF also enhances the chemoselectivity as highlighted in Figure 1 and 4. Starting from 67 % selectivity with respect to the CP products observed for pristine Ru-MOF, the number gradually increases to 85 % in the (0/30) sample almost matching the 87 % from the Ru^{II,III}-MOF. This observation led us to conclude that axial acetate ligands on

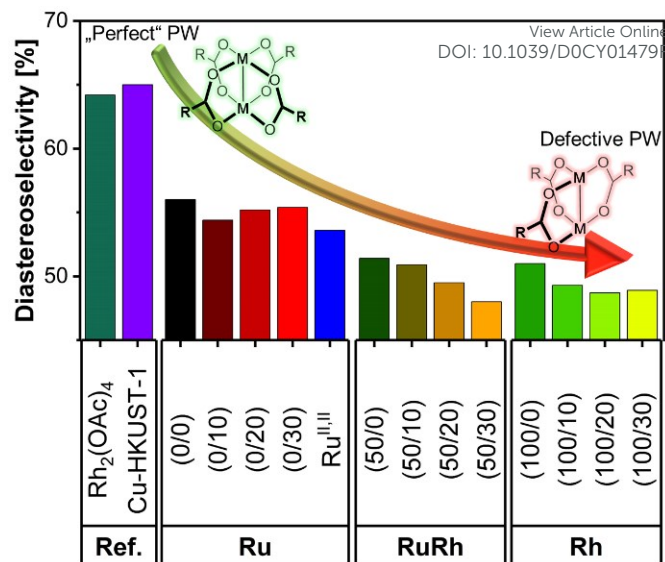


Figure 5: Diastereoselectivities of PW systems studied herein after 4h. The progressive decrease in diastereoselectivity can be correlated with the assumed structural changes with increasing defectiveness of the PWs as indicated schematically. The trend is visible in the order Cu \gg Ru $>$ RuRh $>$ Rh as well as upon increasing TDE.

mixed-valent Ru-PWs are the main source for the undesired homocoupling side products as they are successively removed during TDE. In other words, thermally induced axial ligand removal and the subsequent metal reduction correspond with improved selectivities towards the desired cyclic products for Ru-BTC.

In contrast, both Rh- and RuRh-MOF samples exhibit rather constant activities irrespective of the postsynthetic defect generation. Although, the obtained data suggest a slight drop of activity for low defect amounts (samples (50/10) and (100/10) as shown in Figure 3), the values observed for higher amounts rise again. This intermediate drop could potentially arise from particle agglomeration during TDE responsible for a first drop. Further thermal treatment, however, recreates the catalytic performance as more OMS are generated. No impact on the chemoselectivity of Rh- and RuRh-MOF is observed. This suggests that the nature and the environment of the active Rh sites are apparently not affected by the thermal treatment. Interestingly, any increase in the linear side products that would be expected for a higher number of defective PWs is not substantiated. This is in line with results from CO probe FT-IR measurements that do not suggest large amounts of partially reduced Rh nodes while strong bands for reduced Ru-sites can be observed.³¹

Focusing on the diastereoselectivities of all TDE-MOFs, the slight preference of the *trans*-CP observed for Ru-MOF ($\approx 57:43$) is reduced to 53:47 ($\pm 1\%$) for Ru^{II,III}-MOF. Similar trends of equality of diastereoisomers can be observed for the mixed-metal RuRh- as well as the pure Rh-MOF. Respective graphs are displayed in Figure 5 for 4h reaction time. TDE-MOF samples follow the trend of reduced stereo control as described for the pristine MOFs. From these data we conclude the progressive formation of defective, modified PWs during TDE.

Reference experiments have been performed with Cu-BTC, nanoparticles of Ru and Rh and molecular Rh₂(OAc)₄. As can be

seen in Figure 3 (bottom graph) and Figures S30-32, Cu-BTC exhibits low activity with a TOF of $\approx 18 \text{ h}^{-1}$. Furthermore, its conversion contained a strong induction period. Expanded investigations with hot filtration (performed after 20 min of stirring the suspensions) revealed the activity of Cu-BTC to mainly rely on leaching which is in contrast to findings in a previous report.²⁶ Compared with the well-known copper analogue, precious group metal-based HKUST-1 derivatives studied herein, though more demanding to synthesize, have significantly higher stability towards water and solvents.^{32, 33, 35} A hot filtration experiment with the most active Ru^{II,III}-MOF confirms catalyst heterogeneity as can be seen in Figure S30. Further, emerging nanoparticles being responsible for the increase in activity upon TDE are clearly ruled out (see Figure 3 and S32) as their activity is in the range of the uncatalyzed background reaction. Note, that the presence and potential catalytic impact of ultra-small NPs / single metal atoms is hard to evaluate due to absence of suitable characterization techniques and is thus without consideration. The Rh₂(OAc)₄ reference sample reaches quantitative conversion already after the addition time (0 min), thus its TOF is experimentally limited to 145 h^{-1} with a chemoselectivity of 100% towards cyclopropanes in a diastereomeric ratio of $\approx 64:36$. This is in accordance with existing literature.⁴³ Confinement effects accounting for the diastereoselectivity trends or the formation of the linear products might be ruled out, since both molecular Rh₂(OAc)₄ and Cu-HKUST-1 produce equally high diastereoselectivities. While any confinement is absent in the former, the latter is isostructural to the PGM-MOFs studied herein.

Reusability (catalyst cycling) experiments were performed using Ru^{II,III}- and Rh^{II,III}-BTC samples. For both activated materials, reduced activities are observed within consecutive runs as no additional catalyst sample activation was performed between two different runs (see Figures S33-34). For the Rh-MOF, the chemoselectivity towards linear products is reduced with progressive cycling which we attribute to increasing saturation of modified PWs. The univalent Ru^{II,III} sample follows the chemoselectivity trends observed during TDE in the opposite direction. This clearly suggests a progressive reoxidation and axial ligation back to mixed-valent Ru^{II,III} species featuring lower activity and chemoselectivity with homocoupling side products being formed again. With respect to the low sample amounts, the structural order is mostly preserved after five consecutive cycles (see Figure S35).

Conclusions

Overall, thirteen different samples of precious group metal (PGM)-based HKUST-1 derivatives including thermal defect-engineered variants thereof have been synthesized, characterized, and applied in the cyclopropanation of styrene with ethyl diazoacetate. All PGM-HKUST-1 analogues (Ru^{II,III}, Ru^{II,III}, Rh^{II,III} and mixed-metal Ru^{II,III}Rh^{II,III}) are good CP catalysts with the pristine Ru^{II,III} being less active compared to Ru^{II,III} or Rh^{II,III} but much more tuneable by thermal defect-engineering (TDE). A doubling of the activity and at the same time

diminished formation of homocoupling side products (fumarate and maleate) by 67% are observed. This improvement is rationalized by the successive metal reduction (creation of more OMS) upon TDE. For both Rh- and RuRh-HKUST-1, TDE did not affect the activity or the chemoselectivity but reduced diastereomeric preference suggests progressive formation of modified PWs. The studied PGM-MOFs have good chemical stability and exhibit no leaching as it is observed for Cu-HKUST-1. Nanoparticles or metal leaching contributing to the catalytic activity are ruled out for the PGM-MOFs studied herein, while the moderate activity of Cu-BTC seems to be governed by leaching species. In light of our findings in the CP reaction (presented herein) and in the dimerization of ethene (studied earlier),³¹ we highlight the potential of TDE for the controlled post-synthetic defect incorporation in MOFs and recommend this process over other DE strategies.

The key message of this conceptual study, however, is to make use of the catalytic CP reaction and its corresponding characteristics (activity, chemo- and diastereoselectivity) as novel analytical probe to study MOFs. The PGM-HKUST-1 analogues investigated herein are promising materials for catalytic applications, but their intrinsically pronounced defectiveness is just one factor contributing to their high compositional and structural complexity. Their characterization is challenging and usually requires a multitude of analytical techniques which often just provide fragmented insights that need to be compiled carefully. In this regard, the well-investigated CP reaction is experimentally easy to conduct and could furnish several analytical indications: The relative number and density of OMS, their chemical nature (perfect vs modified PW), whether axially bound anions are present and consequently the metals' oxidation state and its stability under catalysis conditions. Computational ways to describe the observed phenomena to support the findings presented herein are currently under investigation.

Conflicts of interest

There are no conflicts to declare.

Acknowledgements

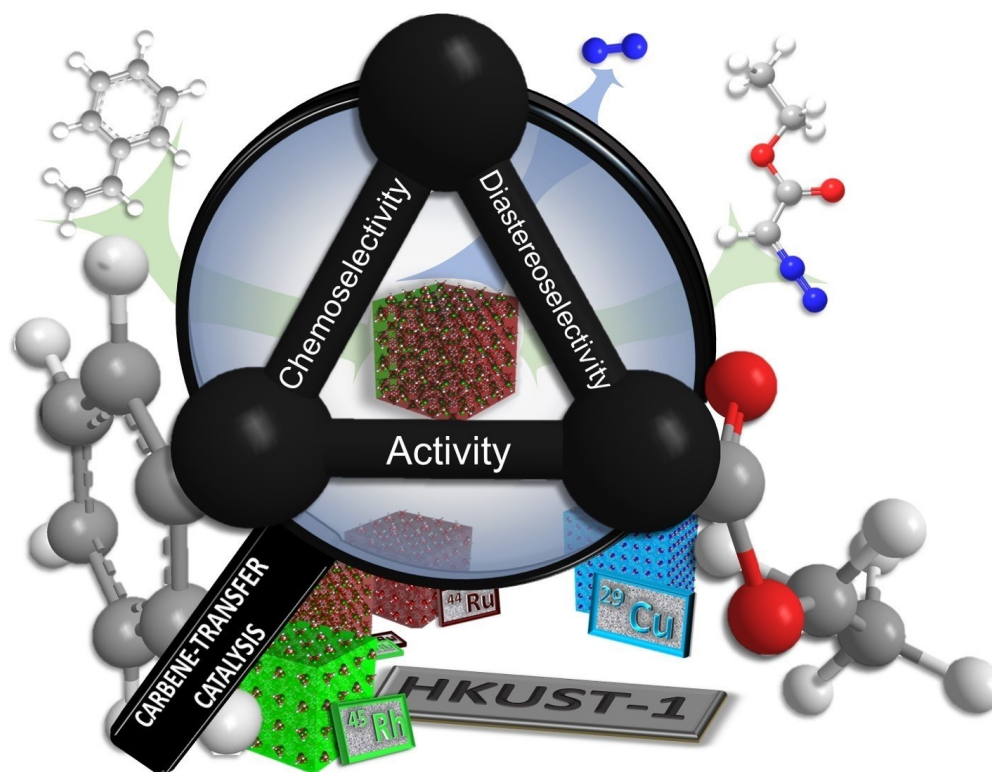
This project was funded by Deutsche Forschungsgemeinschaft grant no. FI-502/32-1 („DEMOFs“). WRH would like to thank TUM Graduate School and GDCh for travel funding. All authors thank Jan Berger, Pia Vervoorts and Dardan Ukaj for experimental support with physisorption measurements and Miryam Gil-Calvo for help with CO titration experiments. WRH thanks Simon Smolders for experimental assistance.

References

1. R. Paulissen, H. Reimlinger, E. Hayez, A. J. Hubert and P. Teyssié, *Tetrahedron Lett.*, 1973, **14**, 2233-2236.
2. A. J. Anciaux, A. J. Hubert, A. F. Noels, N. Petiniot and P. Teyssié, *J. Org. Chem.*, 1980, **45**, 695-702.

3. C. Ebner and E. M. Carreira, *Chem. Rev.*, 2017, **117**, 11651-11679.
4. H. Lebel, J.-F. Marcoux, C. Molinaro and A. B. Charette, *Chem. Rev.*, 2003, **103**, 977-1050.
5. M. Brookhart and W. B. Studabaker, *Chem. Rev.*, 1987, **87**, 411-432.
6. A. Padwa, D. J. Austin, S. F. Hornbuckle, M. A. Semones, M. P. Doyle and M. N. Protopopova, *J. Am. Chem. Soc.*, 1992, **114**, 1874-1876.
7. M. P. Doyle, L. J. Westrum, W. N. E. Wolthuis, M. M. See, W. P. Boone, V. Bagheri and M. M. Pearson, *J. Am. Chem. Soc.*, 1993, **115**, 958-964.
8. M. P. Doyle and D. C. Forbes, *Chem. Rev.*, 1998, **98**, 911-936.
9. M. P. Doyle, *J. Org. Chem.*, 2006, **71**, 9253-9260.
10. M. P. Doyle and D. Ren, in *Prog. Inorg. Chem.*, 2007, DOI: 10.1002/9780470166512.ch2, pp. 113-168.
11. A. F. Noels and A. Demonceau, *J. Phys. Org. Chem.*, 1998, **11**, 602-609.
12. K. Epp, B. Bueken, B. Hofmann, M. Cokoja, K. Hemmer, D. E. De Vos and R. A. Fischer, *Catal. Sci. Technol.*, 2019, **9**, 6452-6459.
13. G. Maas, *Chem. Soc. Rev.*, 2004, **33**, 183-190.
14. F. A. Cotton, K. R. Dunbar and M. G. Verbruggen, *J. Am. Chem. Soc.*, 1987, **109**, 5498-5506.
15. F. Simal, A. Demonceau, A. F. Noels, D. R. T. Knowles, S. O'Leary, P. M. Maitlis and O. Gusev, *J. Organomet. Chem.*, 1998, **558**, 163-170.
16. R. Ye, J. Zhao, B. B. Wickemeyer, F. D. Toste and G. A. Somorjai, *Nat. Catal.*, 2018, **1**, 318-325.
17. X. Cui, W. Li, P. Ryabchuk, K. Junge and M. Beller, *Nat. Catal.*, 2018, **1**, 385-397.
18. Z. Liu, X. Yuan, S. Zhang, J. Wang, Q. Huang, N. Yu, Y. Zhu, L. Fu, F. Wang, Y. Chen and Y. Wu, *NPG Asia Materials*, 2019, **11**, 12.
19. D.-H. Nam, P. De Luna, A. Rosas-Hernández, A. Thevenon, F. Li, T. Agapie, J. C. Peters, O. Shekhah, M. Eddaoudi and E. H. Sargent, *Nat. Mater.*, 2020, **19**, 266-276.
20. B. C. Hodges, E. L. Cates and J.-H. Kim, *Nat. Nanotechnol.*, 2018, **13**, 642-650.
21. D. Farrusseng, S. Aguado and C. Pinel, *Angew. Chem. Int. Ed.*, 2009, **48**, 7502-7513.
22. J. Kim, H.-Y. Cho and W.-S. Ahn, *Catalysis Surveys from Asia*, 2012, **16**, 106-119.
23. J. Liu, C. Fasel, P. Braga-Groszewicz, N. Rothermel, A. S. Lilly Thankamony, G. Sauer, Y. Xu, T. Gutmann and G. Buntkowsky, *Catal. Sci. Technol.*, 2016, **6**, 7830-7840.
24. J. Liu, Y. Xu, P. B. Groszewicz, M. Brodrecht, C. Fasel, K. Hofmann, X. Tan, T. Gutmann and G. Buntkowsky, *Catal. Sci. Technol.*, 2018, **8**, 5190-5200.
25. J. Liu, P. B. Groszewicz, Q. Wen, A. S. L. Thankamony, B. Zhang, U. Kunz, G. Sauer, Y. Xu, T. Gutmann and G. Buntkowsky, *J. Phys. Chem. C*, 2017, **121**, 17409-17416.
26. A. Corma, M. Iglesias, F. X. Llabrés i Xamena and F. Sánchez, *Chem. Eur. J.*, 2010, **16**, 9789-9795.
27. J. Canivet, M. Vandichel and D. Farrusseng, *Dalton Trans.*, 2016, **45**, 4090-4099.
28. A. K. Cheetham, T. D. Bennett, F.-X. Coudert and A. L. Goodwin, *Dalton Trans.*, 2016, **45**, 4113-4126.
29. S. Dissegna, K. Epp, W. R. Heinz, G. Kieslich and R. A. Fischer, *Adv. Mater.*, 2018, **30**, 1704501.
30. Z. Fang, B. Bueken, D. E. De Vos and R. A. Fischer, *Angew. Chem. Int. Ed.*, 2015, **54**, 7234-7254. DOI: 10.1039/C5CY01479F
31. W. R. Heinz, I. Agirrezabal-Telleria, R. Junk, J. Berger, J. Wang, D. I. Sharapa, M. Gil-Calvo, I. Luz, M. Soukri, F. Studt, Y. Wang, C. Wöll, H. Bunzen, M. Drees and R. A. Fischer, *ACS Appl. Mater. Interfaces*, 2020, DOI: 10.1021/acsami.0c10721.
32. O. Kozachuk, K. Yusenko, H. Noei, Y. Wang, S. Walleck, T. Glaser and R. A. Fischer, *Chem. Commun.*, 2011, **47**, 8509-8511.
33. W. Zhang, O. Kozachuk, R. Medishetty, A. Schneemann, R. Wagner, K. Khaletskaya, K. Epp and R. A. Fischer, *Eur. J. Inorg. Chem.*, 2015, **2015**, 3913-3920.
34. W. Zhang, K. Freitag, S. Wannapaiboon, C. Schneider, K. Epp, G. Kieslich and R. A. Fischer, *Inorg. Chem.*, 2016, **55**, 12492-12495.
35. W. R. Heinz, T. Kratky, M. Drees, A. Wimmer, O. Tomanec, S. Günther, M. Schuster and R. A. Fischer, *Dalton Trans.*, 2019, **48**, 12031-12039.
36. J.-L. Zhuang, D. Ceglarek, S. Pethuraj and A. Terfort, *Adv. Funct. Mater.*, 2011, **21**, 1442-1447.
37. J. Adams and D. M. Spero, *Tetrahedron*, 1991, **47**, 1765-1808.
38. A. Caballero, A. Prieto, M. M. Díaz-Requejo and P. J. Pérez, *Eur. J. Inorg. Chem.*, 2009, **2009**, 1137-1144.
39. C. G. Espino and J. Du Bois, *Angew. Chem. Int. Ed.*, 2001, **40**, 598-600.
40. M. C. Pirrung and A. T. Morehead, *J. Am. Chem. Soc.*, 1994, **116**, 8991-9000.
41. A. Tudose, A. Demonceau and L. Delaude, *J. Organomet. Chem.*, 2006, **691**, 5356-5365.
42. W. Zhang, O. Kozachuk, R. Medishetty, A. Schneemann, R. Wagner, K. Khaletskaya, K. Epp and R. A. Fischer, *Eur. J. Inorg. Chem.*, 2015, **2015**, 3913-3920.
43. H. M. L. Davies and S. A. Panaro, *Tetrahedron*, 2000, **56**, 4871-4880.

This work highlights the catalytic cyclopropanation and its characteristics as novel analytical tool to investigate complex MOF structures.



376x293mm (96 x 96 DPI)